IEEE Access
Multidisciplinary : Rapid Review : Open Access Journal

SPECIAL SECTION ON OPTICAL WIRELESS TECHNOLOGIES FOR 5G COMMUNICATIONS AND BEYOND

Received July 27, 2017, accepted September 25, 2017, date of publication October 24, 2017, date of current version November 28, 2017.

Digital Object Identifier 10.1109/ACCESS.2017.2765378

CGH for Indoor Visible Light Communication System

SAFWAN HAFEEDH YOUNUS[1], AHMED TAHA HUSSEIN[1], MOHAMMED THAMER ALRESHEEDI[2], AND JAAFAR M. H. ELMIRGHANI[1], (Senior Member, IEEE)
[1]School of Electronic and Electrical Engineering, University of Leeds, Leeds LS2 9JT, U.K.
[2]Department of Electrical Engineering, King Saud University, Riyadh 11451, Saudi Arabia

Corresponding author: Safwan Hafeedh Younus (elshy@leeds.ac.uk)

This work was supported by the International Scientific Partnership Program at King Saud University under Grant ISPP# 0093.

ABSTRACT In this paper, we propose, design, and evaluate two indoor visible light communication (VLC) systems based on computer generated holograms (CGHs); a simple static CGH-VLC system and an adaptive CGH-VLC system. Each transmitter is followed by the CGH, and this CGH is utilized to direct part of the total power from the best transmitter and focus it to a specific area on the communication floor. This leads to reduction in inter-symbol interference and increasing in the received optical power, which leads to higher data rates with a reliable connection. In the static CG11H-VLC system, the CGH generates 100 beams (all these beams carry same data) from the best transmitter and directs these beams to an area of 2 m × 2 m on the communication floor. In the adaptive CGH-VLC system, the CGH is used to generate eight beams from the best transmitter and steer these beams to the receiver's location. In addition, each one of these eight beams carries a different data stream. Whereas in the first system, a single photodetector is used (added simplicity), an imaging receiver is used in the second one to obtain spatial multiplexing. We consider the lighting constraints where illumination should be at acceptable level and consider diffusing reflections (up to second order) to find the maximum data rate that can be offered by each system. Moreover, due to the fact that each beam in the adaptive CGH-VLC system conveys a different data stream, co-channel interference between beams is taken into account. We evaluate our proposed systems in two different indoor environments: an empty room and a realistic room using simple on–off-keying modulation. The results show that the static CGH-VLC system offers a data rate of 8 Gb/s while the adaptive CGH-VLC system can achieve a data rate of 40 Gb/s.

INDEX TERMS Computer generated hologram, static CGH-VLC system, adaptive CGH-VLC system, inter-symbol interference, co-channel interference, on-off-keying.

I. INTRODUCTION

Over the past decade, visible light communication (VLC) systems have become very attractive; due to using energy efficient light emitting diodes (LEDs) for illumination and data communication. In addition, the saturated spectrum of the conventional radio frequency (RF) systems makes many researchers focus on VLC systems. In terms of lighting, LEDs have several advantages compared with traditional lighting sources (incandescent and fluorescent), such as longer lifetime, lower power consumption and higher luminance efficiency. Moreover, LEDs can be used for both illumination and data communication, while traditional lighting sources are used for illumination only [1]. In terms of data communication, VLC systems have numerous advantages compared with RF systems, such as abundant bandwidth, better security, and the availability of simple front-end devices at low cost [2].

VLC systems are still under development and several challenges face these systems, especially in terms of achieving high data rates and using the VLC spectrum efficiently. The main challenges facing high data rate VLC systems are the low modulation bandwidth of the LEDs (typically several megahertz for the blue-chip LED and a few hundred megahertz for the RGB LED) [3] and the inter-symbol interference (ISI) caused by multipath propagation, which limits the data rates in VLC systems [4].

Many directions have emerged to increase the data rate associated with LEDs based VLC systems. One direction is to use an equalizer at the transmitter and/or the receiver with a simple modulation scheme (for example on-off keying, OOK) with blue-chip LEDs [5]–[7]. However, the loss in the electrical signal to noise ratio (SNR) can be high. For example, in one such system, it was 18 dB due to the equalizer and 36 dB due to blue filter [3], which leads to a negative effect on the illumination level and reduction in the distance supported between the transmitter and the receiver. The other trend is to use multiple input multiple output (MIMO) techniques and complex modulation to increase the data rate in the VLC system [8]–[10]. A good enhancement in the data rate was achieved by using wavelength division multiplexing (WDM) with red, green and blue (RGB) LEDs [11]–[13]. However, the data rates achieved are still low compared with the available VLC spectrum.

Another approach to enhance the data rate in VLC systems is to use laser diodes (LDs) instead of LEDs, due to the higher modulation bandwidth of LDs compared with LEDs. A commercial high power RGB LD has been used to achieve a 4 Gb/s data rate at room temperature [14]. A data rate up to 6.52 Gb/s was achieved using an LD based remote phosphor technique with orthogonal frequency division multiplexing (OFDM) and an adaptive loading method [15]. In [16], multicolour LDs in conjunction with WDM method and imaging diversity receiver (IMDR) were used to obtain 10 Gb/s for an indoor VLC system. A number of design approaches have been proposed with WDM and parallel streams to determine the abilities of LDs in terms of achieving data rates up to 100 Gb/s [17]. LDs and imaging receiver have been studied in conjunction with a delay adaptation technique to achieve 10 Gb/s in a realistic room [4].

Optical beam steering is a technique that can be used to focus an optical power source on a specific target. One of the main challenges in VLC systems when working at high data rates (several Gb/s) is multipath propagation, which leads to increase in the ISI and consequently degrades the system performance. Thus, by using the beam steering, the 3-dB channel bandwidth is enhanced, since part of the total power is focused on the receiver, which reduces the effect of multipath propagation. Beam steering is widely investigated in optical wireless communication. In infrared (IR) systems, beam steering has been used to optimize the distribution of the diffusing spots, which leads to improving the received optical power [18], [19]. Beam steering has also been studied in VLC system to improve the SNR and increase the data rate [20]–[22]. A significant improvement in the VLC system data rate (20 Gb/s) was achieved by employing LDs, imaging receivers, beam steering and computer generated holograms (CGHs) [21].

The aim of this paper is to propose and design an optical indoor system based on CGH. Two indoor VLC systems are proposed: static (low complexity) CGH-VLC system and adaptive CGH-VLC system. In an indoor VLC system, many transmitters (LEDs or LDs) with broad beams are employed to obtain an acceptable level of lighting in the room. Thus, the channel in indoor VLC systems includes many line-of-sight (LOS) components that arrive at an optical receiver with different delays, and consequently induce ISI at a high data rate. In addition, multipath propagation results in optical signals reaching an optical receiver through reflections from reflective surfaces of a room leading to pulse spreading and significant ISI. Therefore, just one light unit is used at any given point in time to transmit data in this work. This is the unit that has the strongest connection with the optical receiver. This, however, leads to decrease in the received optical power. Hence, each light unit is followed by a CGH, and this CGH is used to direct part of the total power of the best light unit and focus it on a specific area on the communication floor of the room.

It should be noted that in [21], the CGH was used to generate one beam and steer it to the optical receiver. However, in this paper, for the static CGH-VLC system, the CGH is used to generate multiple broad fixed beams and direct them to a 2 m × 2 m area on the communication floor under the best light unit, while CGH is used in the adaptive CGH-VLC system to generate multiple narrow beams and steer them to the optical receiver.

In the static CGH-VLC system, the CGH is utilized to direct 30% of the total power of the best light unit. It generates 100 beams (all generated beams carry the same data) and focuses these beams on an area of 2 m × 2 m. Thus, in this system, no beam steering is required. On the other hand, in the adaptive CGH-VLC system, the adaptive CGH is used to direct a 20% of the total power of the best transmitter towards the receiver. It generates eight beams (each beam conveys a different data stream) and steers these beams to the optical receiver. The 30% and 20% values of the total power of the best light unit are chosen to ensure that the illumination level stays at an acceptable level while directing the maximum possible power towards the receiver. To obtain spatial multiplexing in the adaptive CGH-VLC system, an imaging receiver with 288 pixels (12 × 24) is used while a single photodetector is used with the static CGH-VLC system. In this work, we used LDs as a source of illumination and data communication, which offers high modulation bandwidth compared with LEDs. We investigate our proposed systems in two different room scenarios in the presence of diffuse reflections (up to second order): an empty room and a realistic environment room with a door, windows, bookshelves, mini cubicles and other objects. The results showed that the static CGH-VLC system has the ability to offer a high data rate up to 8 Gb/s while the adaptive CGH-VLC system achieves a data rate of 40 Gb/s (8 beams × 5 Gb/s for each beam) with simple OOK modulation.

The remainder of this paper is organized into sections as follows: Section II describes the room setup and LDs-light units' configuration. Section III presents the receivers configurations. Section IV describes the design of the CGH. The configuration of the static CGH-VLC system is given in Section V. Section VI explains the design of the adaptive CGH-VLC system. Simulation results and discussion of the proposed systems are given in Section VII. Finally, conclusions are drawn in Section VIII.

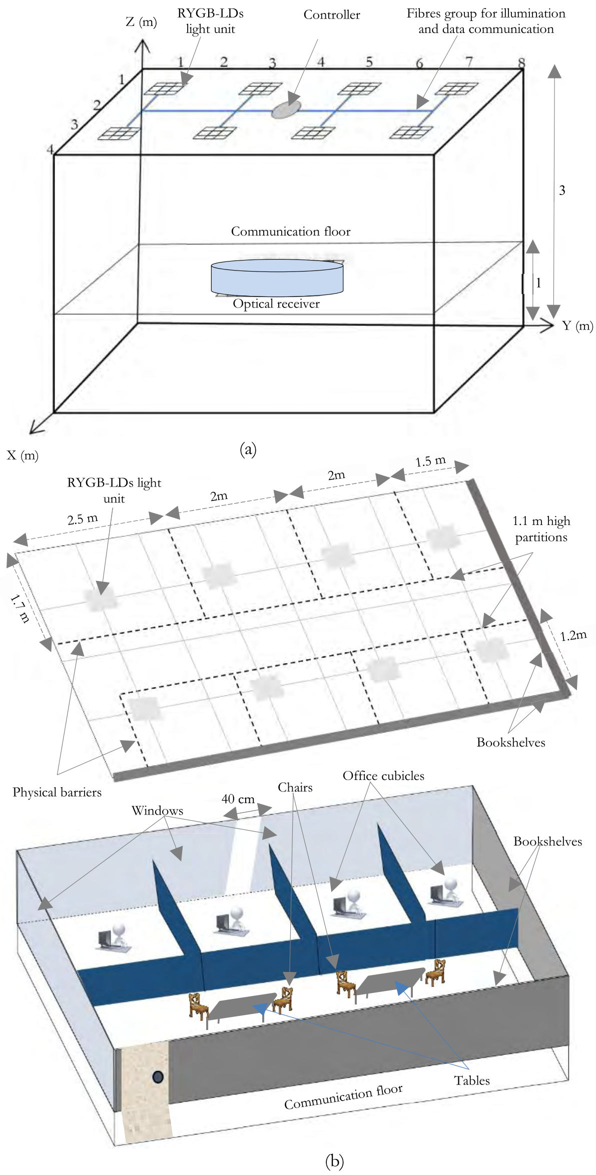

FIGURE 1. **(a) An empty room (room A) and (b) a realistic room (room B).**

II. VLC ROOM SETUP

Two room configurations were used in the analysis. An empty room (room A) that has neither doors nor windows and a realistic room (room B) that has a door, windows, bookshelves and physical partitions as shown in Fig. 1 (a) and (b), respectively. The dimensions of rooms A and B were 4 m × 8 m × 3 m (width × length × height) with reflection coefficients of 0.3 for the floor and 0.8 for the ceiling and walls [23]. Room B, which represented a small office, has a door, three large windows, bookshelves, furniture, chairs, desks, tables and mini cubicle offices as shown in Fig. 1 (b). The reflection coefficients of the door and three windows were set to zero, which means that they reflect no signals.

In addition, the two walls ($x = 4$ m and $y = 8$ m) in room B are covered with bookshelves and filling cabinets (see Fig. 1 (b)) and have a 0.4 reflectivity [24]. The mini cubicle office partitions were assumed to either absorb or block the signal. Furthermore, the reflection coefficients of the desks, chairs and tables inside room B were set to 0.3 (similar to the roof). The physical partitions and low reflective objects in room B created shadowing, which leads to increased complexity in room B.

The walls, ceiling and floor were modelled as Lambertian reflectors, where experimental measurements have shown that plaster walls are roughly Lambertian reflectors [23]. A ray tracing algorithm was used to model the reflections; thus, room A and room B were divided into a number of equal square-shaped surface elements with an area of d_A and reflection coefficient of ρ. Each surface element was treated as Lambertian source with $n = 1$, where n is the Lambertain emission order. To obtain results with high resolution, the size of the surface element should be very small, but the computation time increases exponentially. Thus, to keep computations within a reasonable time, a 5 cm × 5 cm size was chosen for the surface element in the first order reflections and 20 cm × 20 cm size for second order reflections. In this work, up to second-order reflections were considered in the simulation; at a high data rate second-order reflections have a great impact on VLC systems. Previous research has found that most of the received power is within the first and second order reflections but that when it goes beyond the second order signals are highly attenuated [25]. Therefore, reflections up to the second order are considered in this work.

In this paper, LDs were used rather than LEDs to achieve multi-gigabit data rates while employing a simple modulation technique (OOK). Recent research has shown that LDs are much brighter than LEDs and have output powers (several watts) more than LEDs, which leads to high lumen output [26]. Moreover, an experimental test showed that lighting based on multicolour LDs can operate without any effects on the human eye [27]. Therefore, we used the same specifications of the red, yellow, green and blue (RYGB) LDs that were used in [27]. In our simulation, eight RYGB LDs-light units were used for illumination and were installed on the ceiling (along the x-y axis) of the room (3 m above the floor). In addition, the eight RYGB LDs-light units were distributed on the ceiling as shown in Fig. 1 (a) to achieve an acceptable illumination level in the room, which ensures the ISO and European illumination requirements were met [28]. Each RYGB LDs-light unit had 9 RYGB LDs (3 × 3) with a separation of 3 cm. To calculate the illumination level, each RYGB LD was assumed to have a Lambertian radiation pattern. Therefore, the LOS illumination can be obtained at a point (x, y) following [4], [29]:

$$E_{LOS} = \frac{I\,(0)\,cos^{n}\,(\theta)\cos(\Upsilon)}{R_1^2} \tag{1}$$

where I (0) is the centre luminous intensity of the RYGB LD, θ is the irradiance angle, R_1 is the distance between the RYGB LD and any point in the floor, Υ is the angle of incidence and

n is the Lambertion emission order as defend in [30]:

$$n = -\frac{\ln(2)}{\ln\left(cos\left(\Phi_{\frac{1}{2}}\right)\right)} \quad (2)$$

where $\Phi_{\frac{1}{2}}$ is the semi angle at half power of the RYGB LD. In this work, we considered reflections up to second order; hence, calculations of first and second order reflections of the illumination can be found in [4] and [31].

The coordinates of the RYGB LDs-light units were (1 m, 1 m, 3 m), (1 m, 3 m, 3 m), (1 m, 5 m, 3 m), (1 m, 7 m, 3 m), (3 m, 1 m, 3 m), (3 m, 3 m, 3 m), (3 m, 5 m, 3 m), and (3 m, 7 m, 3 m), as shown in Fig. 1 (a). Each RYGB LDs-light unit followed the CGH, which was used to focus a portion of the total power of the RYGB LD toward a target [21].

III. RECEIVERS CONFIGURATION

Two receivers were used in this work: a single photodetector receiver and an imaging receiver. The single photodetector receiver was used with static CGH-VLC system, which is the most basic receiver configuration and has been widely investigated. The photosensitive area of the single photodetector was chosen to be 0.5 mm^2 to decrease the internal capacitance of the photodetector and enable the photodetector to operate at high data rates while collecting significant optical power as shown in the results section. For a silicon photodetector, the bandwidth of the single photodetector receiver given as [32]:

$$BW = \frac{1}{2\pi R_l C_d} \quad (3)$$

where R_l is the load resistor and C_d is the photodetector's capacitance which is proportional to the photosensitive area of the photodetector and can be given as [33]:

$$C_d = \frac{\varepsilon_0 \varepsilon_r A}{w} \quad (4)$$

where A is the photodetector's area and w is the detector thickness ($w = 100\ \mu$m). A value of R_l equal to 50 Ω leads to matching between the photodetector and the preamplifier [32]. Thus, the maximum band width of this photodetector is $\sim$ 6.18 GHz, which can receive data at rates up to 8.83 Gb/s since the bandwidth needed is 0.7 times the bit rate for OOK modulation [34]. To reduce the multipath dispersion and pulse spread, a narrow field-of-view (FOV) should be selected. However, this FOV should be chosen to ensure that the photodetector views at least one RYGB LDs-light unit at any location on the communication floor of the room. Therefore, the FOV of the single photodetector was selected to be equal to 40°, which ensures that the receiver will see at least one RYGB LDs-light unit when it is placed at the room centre (2 m, 4 m, 1 m) as the distance between the transmitters and the receiver become maximum at this location.

An imaging receiver was used in the adaptive CGH-VLC system rather than the single receiver to achieve spatial multiplexing. The main advantages of using an imaging receiver are: 1) one concentrator is used for all photodetectors, which reduces the size and the cost of the receiver and 2) the ability to realize a large number of pixels in a single planner array of photodetectors [35]. In addition, the imaging receiver in the VLC system mitigates the delay spread because each pixel in the imaging receiver receives a limited range of rays (each pixel has a narrow FOV), which leads to an increase in the channel bandwidth and increase in the SNR [25]. In the imaging receiver, all photodetectors were laid out as a single detector segmented into J equal-sized rectangular-shaped elements with no gaps between them. Therefore, the signal fell on no more than four pixels [36]. Thus, the area of each pixel was equal to the area of the photodetector divided by the number of pixels. The imaging receiver in this work has 288 (12 × 24) pixels. In addition, the lens was used as a concentrator to collect and concentrate the light from a large area down to a smaller detector area as shown in Fig. 2. In our analysis, we employed the lens that was used in [35]. The diameter of the entrance aperture of the lens is equal to 3 cm; thus, the entrance area of the lens was $A = \frac{9\pi}{4}$ cm^2 with exit area $A' = \frac{Asin^2(\psi)}{N^2}$, where N is the refractive index ($N = 1.7$) and ψ is the acceptance angle of the lens ($\psi < 90°$). The gain of the lens is:

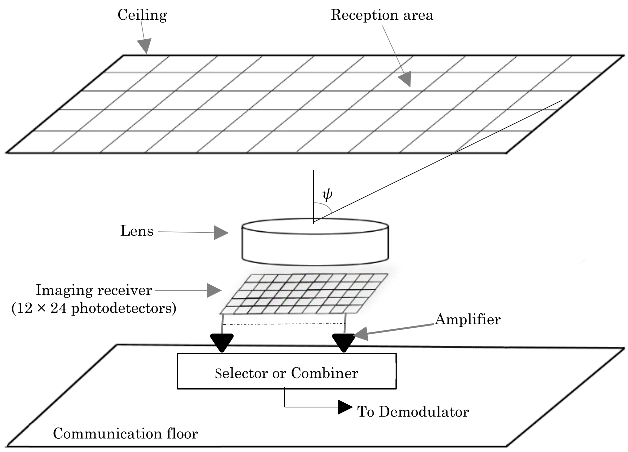

FIGURE 2. Imaging receiver physical structure.

$$g(\psi) = \frac{N^2}{sin^2(\psi)} \quad (5)$$

The transmission factor of the imaging concentrator is given by [35]:

$$T_c(\delta) = -0.1982\delta^2 + 0.0425\delta + 0.8778 \quad (6)$$

where δ is the incidence angle measured in radians. The acceptance angle of the concentrator (ψ) was chosen as 65° so that the imaging receiver viewed the whole ceiling when it was located at the centre of the room. In addition, the size of the detector array was selected equal to the exit area of the concentrator. Therefore, the photosensitive area of the detector used in this work was 2 cm^2 (1 cm along the x-axis and 2 cm along the y-axis) and the area of each pixel was 0.69 mm^2. Each pixel in the imaging receiver could amplify the photocurrents received separately (see Fig. 2), thus different methods can be used for processing, such as select the best (SB), equal gain combining (EGC) or maximum ratio combining (MRC) techniques [18], [35]. In our analysis, the single photodetector and the imaging receiver were placed 1 m above the floor, which represents the communication floor as shown in Fig. 1 (a).

The imaging receiver could see the whole ceiling when it was located at the room center; thus, the ceiling was divided into small divisions called reception areas, as shown in Fig. 2. In our design, the ceiling was divided into 288 reception areas, and each reception area was cast onto a single pixel. The reception area was found (when the receiver was at the room center) based on the reception angles along the x-axis (α_x) and y-axis (α_y) directions with respect to the receiver's normal vector, see Fig. 3. The reception angles can be calculated as:

$$\alpha_x = tan^{-1}\left(\frac{d_x}{h}\right) \text{ and } \alpha_y = tan^{-1}\left(\frac{d_y}{h}\right) \quad (7)$$

where d_x is the x-axis horizontal separation, d_y is the y-axis horizontal separation and h is the reception area height as shown in Fig. 3.

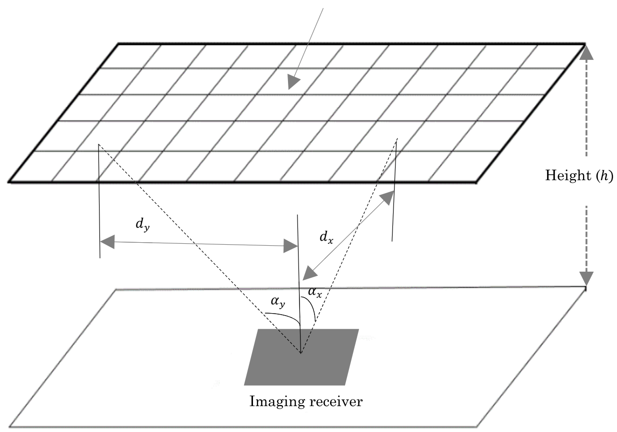

FIGURE 3. **Reception areas associated with the pixels when the imaging receiver is located at the room center (2 m, 4 m, 1 m).**

When the receiver is located at the room center, all reception areas are located on the ceiling. However, when the receiver moves along the x-axis and/or y-axis, some of the reception areas on the ceiling start to appear on the walls. Fig. 4 shows that some of the reception areas start to appear on X-Z wall and Y-Z wall when the receiver is located at the room corner (1 m, 1 m, 1 m). Thus, when the receiver starts moving the new reception areas should be calculated with respect to the height of the center of the reception areas above the communication floor on the X-Z wall (Z_x) or on the Y-Z wall (Z_y) (see Fig. 4) as [4], [18]:

$$Z_x = \frac{X_r}{\tan(\alpha_x)} \text{ and } Z_y = \frac{Y_r}{\tan(\alpha_y)} \quad (8)$$

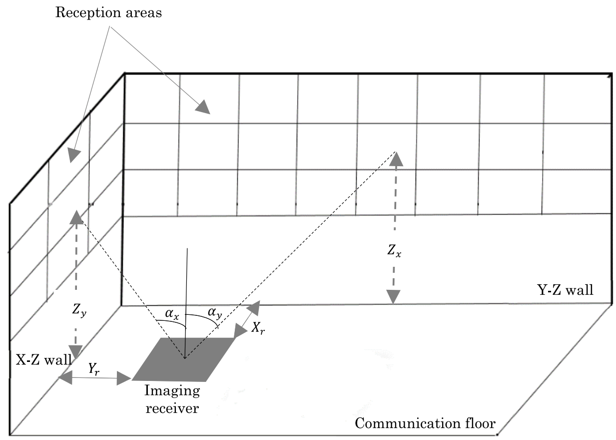

FIGURE 4. **Reception areas associated with the pixels when the imaging receiver is located at the room corner (1 m, 1 m, 1 m).**

where X_r is the horizontal separation distance between the imaging receiver and the Y-Z wall and Y_r is the horizontal separation distance between the imaging receiver and the X-Z wall as shown in Fig. 4.

Based on the area of the pixel, the maximum bandwidth of each pixel of the imaging receiver is $\sim$ 4.48 GHz, which supports data rates up to 6.35 Gb/s.

IV. CGH FOR INDOOR VLC SYSTEM

In VLC systems, many light units, which are spatially separated, are installed in a room ceiling to obtain the required illumination level. However, for a data communication, this means that many LOS components reach the optical receiver with different times of arrival, which leads to ISI at high data rates. Therefore, just one RYGB LDs-light unit is used to transmit a data for a given receiver position. This is the unit that has the best SNR for the given optical receiver location. However, this leads to decrease in the received optical power. Thus, each RYGB LDs light unit was followed by a CGH, which is an optical device that can be used to modulate the phase and the amplitude of the light on each pixel [20]. The CGH is utilized to direct part of the total power of the best RYGB LDs-light unit and focus it on a specific area on the communication floor of the room. In addition, use of the CGH leads to a reduction in multipath propagation.

The CGH can produce spots with any prescribed amplitude and phase distribution. Computing the CGH means the calculation of the complex transmittance of the CGH as given [24]:

$$H(u,v) = A(u,v)\, e^{j(u,v)} \quad (9)$$

here $A(u, v)$ is the amplitude distribution of the hologram, $\Phi(u, v)$ is the hologram's phase distribution and (u, v) are coordinates in frequency space. The CGH has the ability to modulate the amplitude and/or the phase of an incoming wavefront. The CGH is used to direct a part of the total power of the best light unit and focus it into a specific area. Thus, the hologram used modulates only the phase of the incoming wavefront, which makes the transmittance amplitude equal to unity. Diffraction theory is used to compute the distribution of the beams and this is encoded into a hologram [37] in which the phase of each pixel in the CGH will be optimized to obtain the desired far-field pattern. The hologram $H(u, v)$ is in the frequency domain and the location of each pixel in the hologram is defined by the frequency coordinates u and v whereas the observed diffraction pattern (reconstruction far field pattern in the communication floor) is in the spatial domain. Therefore, there are two domains, the CGH domain and the far-field pattern domain, and a Fourier transform is used to establish the relationship between them as [38]:

$$h(x, y) = \iint H(u, v)\, e^{-j2\pi(ux+vy)} dx\, dy \qquad (10)$$

The hologram has an $M \times N$ array of rectangular cells and each cell has a size of R $\times$ S with complex transmittance value H_{kl} : $-M/2k \leq M/2$ and $-N/2l \leq N/2$ [24]. Consequently, the diffraction pattern is given as [38]:

$$h(x, y) = RS\ sinc\left(R_x, S_y\right) \sum_{k=-\frac{M}{2}}^{\frac{M}{2}-1} \sum_{l=-\frac{N}{2}}^{\frac{N}{2}-1} \times H_{kl}\, e^{j2\pi(Rxk+Syl)} \qquad (11)$$

Due to the finite resolution of the output device, the cost function (CF) was defined as the difference between the desired far-field pattern and the actual output pattern. In this paper, simulated annealing algorithm was used to optimize the output of the CGH where the phase of the CGH gradually changed to obtain the desired far-field pattern [39]. The distribution of the pattern in the far field is $f(x, y) = |f(x, y)|\, e^{j\Phi(x,y)}$. The target of the design is to obtain the distribution of the CGH $g(v, u)$ that generates a reconstruction $g(x, y)$ as close as possible to the desired distribution $f(x, y)$. The CF is a mean square error that corresponding to the difference between the normalized desired object energy $f''(x, y)$ and the scaled reconstruction energy of the kth iteration $g''(x, y)$ as [21]:

$$CF_k = \sqrt{\sum_{i=1}^{M} \sum_{j=1}^{N} \left(|f''(x, y)|^2 - |g''(x, y)|^2\right)^2} \qquad (12)$$

V. STATIC CGH-VLC SYSTEM DESIGN

Only one RYGB LDs-light unit is utilized to transmit the data. Thus, select the best algorithm (SBA) was used to select the best (RYGB LDs-light unit) transmitter, which gives an optimum link between the transmitter and the receiver. The SBA can be used to find the optimum link according to the following steps:

1) The controller gives an ID to each RYGB LDs-light unit.
2) The controller activates one of the RYGB LDs-light units to send a pilot signal.
3) SNR is calculated at the receiver side.
4) The user transceiver sends (using an IR beam) a low data rate control feedback signal to inform the controller of the SNR associated with the first RYGB LDs-light unit. The design of IR uplink has been investigated in [40].
5) Repeat steps 2 to 4 for other RYGB LDs-light units.
6) The RYGB LDs-light unit that yields the best SNR is chosen by the controller.
7) The controller activates a silent mode for the remaining seven transmitters and keeps the best RYGB LDs-light unit 'ON' (in the communications sense) to send the information signal.

The SNR of each RYGB LDs-light unit relies on the distance between the RYGB LDs-light unit and the optical receiver. Thus, in some locations, two or more RYGB LDs-light units may have the same SNR. In this case, the controller selects one of them and discards the others. In addition, due to switching ON the RYGB LDs-light units individually, there was no interference between the signals transmitted from the RYGB LDs-light units. Thus, the SNR of each RYGB LDs-light unit was obtained without CCI. The SBA algorithm is given in Table 1.

TABLE 1. SBA Algorithm.

Inputs: N =8; (Number of RYGB LDs-light units)

for k =1: N;
  Calculate and sum the received powers
  Produce the impulse response $h_m(t)$
  Calculate $(P_{S1} - P_{S0})$
  Compute $SNR_k = \left(\frac{R(P_{S1}-P_{S0})}{\sigma_t}\right)^2$
end for
$SNR_{max} = max\ (SNR_k)$
Select RYGB LDs-unit that yields SNR_{max}

In the static CGH-VLC system, we used a static CGH in which the CGH generates multiple fixed beams without beam steering towards the receiver. Therefore, the size and the number of the beams should be selected to cover all possible locations of the receiver on the communication floor and the amount of power used by these beams and their spatial organization should not affect the illumination level. Although selecting beams with small sizes offers high received power, this leads to a reduction in the coverage area of the CGH (gaps between generated beams) and restrict the mobility of the user. On the other hand, beams with large sizes lead to increase in the coverage area of the CGH, but this offers low received power. Thus, an optimum size of the beam should be selected. Due to the distribution of the RYGB LDs-light units on the ceiling of the room, the communication floor of the room was divided into eight small areas with an area of 2 m $\times$ 2 m each as shown in Fig. 4. One RYGB LDs-light unit transmits the data for the given receiver location. The static CGH generates 100 (10 $\times$ 10) beams and focuses them on this small area (see Fig. 5). For example, if the size of the beam is 20 cm, this will cover an area of 2 m $\times$ 2 m (2 m $\times$ 2 m/ 20 cm $\times$ 20 cm = 100). However, this will leave gaps between adjacent beams. Thus, a beam diameter of 30 cm is used to eliminate the gaps between

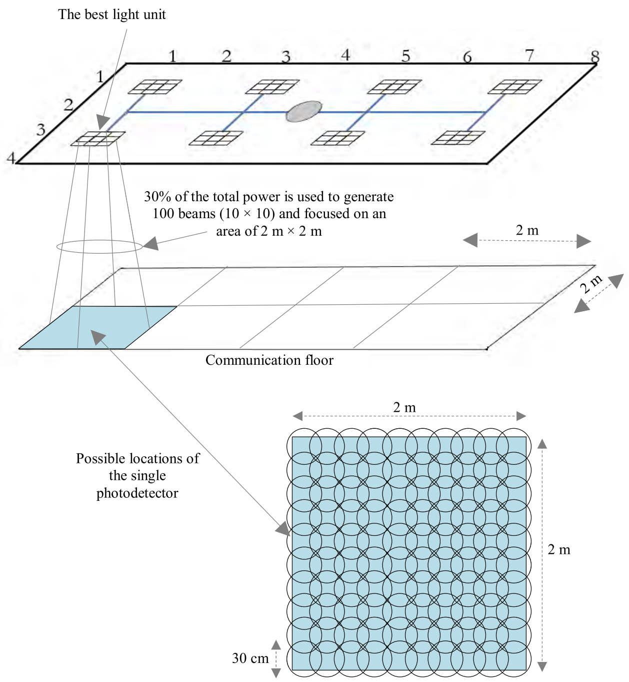

FIGURE 5. Configuration of the static CGH.

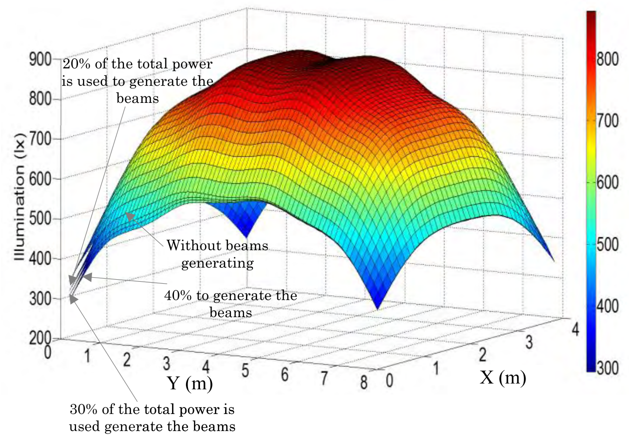

FIGURE 6. The distribution of illumination of the static CGH-VLC system on the communication floor, without CGH beams, minimum illumination 342 lx and maximum illumination 878 lx. When 20% of the power is used to generate the CGH beams, the minimum illumination becomes 318 lx and the maximum illumination becomes 874 lx. When 30% of the power is used to generate the CGH beams, the minimum illumination becomes 306 lx and the maximum illumination becomes 870 lx and for the 40% the case the minimum and the maximum illumination become 291 lx and 865 lx respectively.

adjacent beams. However, some of the beams (beams near to the walls) will hit the walls and increase diffusing reflections. It should be noted that all the beams generated by the static CGH carry the same data. In addition, the single photodetector was used with this system.

In this work, we considered the required illumination level in the room. Thus, to calculate the amount of power that can be taken from the best RYGB LDs-light unit by the CGH without affecting illumination level in the room, we investigated different values such as 20%, 30% and 40% of the total power of the best transmitter. We examined these values while considering the RYGB LDs-light unit located at the room's corner (i.e. the coordinate of the best transmitter is 1 m, 1 m, 1 m) as the lowest illumination occurs at the corners of the room. The results showed that a maximum of 30% of the total power of the RYGB LDs-light unit can be used by the CGH to generate beams and focus them on the 2 m × 2 m area without reducing the illumination under the minimum level required by the illumination standards (i.e. 300 lx [28]). Fig. 6 shows the distribution of the illumination level on the communication floor of the room. It can be seen that without generating the beams, the minimum lighting value is equal to 342 lx, which achieves sufficient illumination in the room (i.e. more than 300 lx). The minimum lighting levels when using 20%, 30% and 40% of the total power of the best transmitter are equal to 318 lx, 306 lx and 291 lx respectively. Thus, 30% of the total power of the best light unit was selected to keep the illumination at an acceptable level.

VI. DESIGN OF THE ADAPTIVE CGH-VLC SYSTEM

Although more complex, additional enhancements (such as increasing the received optical power and reduce the effect of ISI) in the indoor VLC system can be obtained by steering multiple beams of light from the best RYGB LDs-light unit towards the optical receiver. Thus, in the adaptive CGH-VLC system, the CGH was used to generate multiple beams from the best RYGB LDs-light unit and direct these beams to the optical receiver (see Fig. 7); hence, the exact location of the optical receiver should be obtained. We used the imaging receiver with the adaptive CGH-VLC system, which enables each beam from each RYGB LD in the best RYGB LDs-light unit to carry a different data stream, received by a different pixel. The effect of the CCI was taken into account in this system. The number of the optimum beams that should be generated by the CGH at a specific data rate will be explained later. Due to directing all beams towards the optical

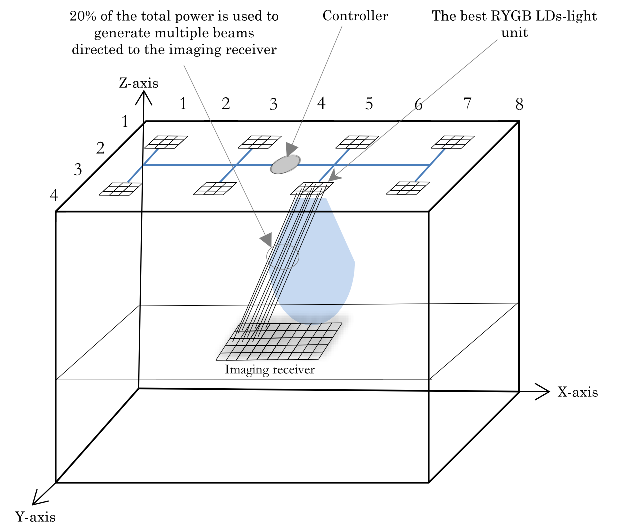

FIGURE 7. Configuration of the adaptive CGH-VLC system.

receiver, the CGH used only 20% of the total power from each RYGB LD in the best RYGB LDs-light unit to generate the beams. The 20% value was selected to ensure that the illumination level stayed at an acceptable level. The following algorithms were used to design the adaptive CGH-VLC system:

A. SELECT THE BEST ALGORITHM (SBA)

In this system, we used the same algorithm that was presented in the static CGH-VLC system to find the best transmitter. However, here the SNR is estimated at each pixel of the imaging receiver and the controller selects the number of the pixel (the best pixel) that gives the best SNR at each step.

B. POSITION IDENTIFICATION ALGORITHM (PIA)

A PIA algorithm was introduced to identify the location of the receiver. Each RYGB LDs-light unit can find the location of the receiver via searching the area underneath it (2 m × 2 m), which reduces the time to find the receiver's location. The RYGB LDs-light unit that was chosen in the SBA initially produces a single beam using the CGH and scans it along a number of possible locations in its small area (2 m × 2 m) of the room to find the receiver location. The CGH can be used to change the intensity and the direction of the light beams adaptively, with low complexity [41]. Thus, the best RYGB LDs-light unit followed by the CGH can be used to find the receiver's location by generating a directional beam to scan possible locations of the receiver in the small area (2 m × 2 m). The locations of the generated beam can be altered by changing the transmission angles of the CGH along the x-axis (θ_x) and along the y-axis (θ_y) with respect to the transmitter's normal vector. In this work, we used a divide and conquer (D&C) algorithm to find the receiver's location. In this algorithm, the possible location areas were divided into four sub-divided areas, and in each area, the CGH produced a single beam and scanned it with a step angle (θ_{step}) along the x-axis and y-axis in the sub-divided area. The sub-divided area that had the best SNR was chosen as the new possible location area, and it was divided into another four sub-divisions. In this work, eight iterations were carried out to find the exact location of the receiver. The PIA determined the receiver location according to the following steps:

1) Set up the initial parameters of the CGH in the best RYGB LDs-light unit to define the boundary scan of the small area (2 m × 2 m). These parameters were the transmission angles along the x-axis ($\theta_{x\text{-}start}$ to $\theta_{x\text{-}end}$) and the transmission angles along the y-axis ($\theta_{y\text{-}start}$ to $\theta_{y\text{-}end}$) with respect to the transmitter's normal vector. The transmission angles in the xy-axes are configured to vary between $-26.6°$ and $26.6°$, which covers the area of 2 m × 2 m along the xy-axes.
2) The scan area (2 m × 2 m) was divided into four sub-areas (quadrants) for the first iteration. The boundary angles associated with the first quadrant were $\theta_{x\text{-}start}$ to 0 and $\theta_{y\text{-}start}$ to 0; the second quadrant angles were $\theta_{x\text{-}start}$ to 0 and 0 to $\theta_{y\text{-}end}$; the third quadrant angles were 0 to $\theta_{x\text{-}end}$ and $\theta_{y\text{-}start}$ to 0 and the fourth quadrant angles were 0 to $\theta_{x\text{-}end}$ and 0 to $\theta_{y\text{-}end}$.
3) A single beam was generated and moved with a step size of 100 cm to scan the four quadrants.
4) The SNR was estimated at each step and the user transceiver sent a control feedback signal at a low data rate to inform the controller of the SNR associated with each step.
5) The controller compares the SNRs recorded with the associated transmission angles θ_x and θ_y that gave the maximum SNR.
6) The controller configured the parameters of the best quadrant for the next iteration and reduce the step size of the beam by a factor of two.
7) It repeats steps 4 to 6.
8) The iterations stop if the step size $\leq$ 1 cm.
9) The controller assigns the optimum location with coordinates (x, y, z) to the transmitter.

It should be noted that in the SBA and PIA, the CGH generated one beam to select the best RYGB LDs-light unit and to find the exact location of the optical receiver. Thus, the calculations of the above algorithms were based on the SNR.

The controller connecting all RYGB LDs-light units is used to accomplish the connection between transmitters and the optical receiver. Thus, it is proposed that the optical receiver re-evaluates its performance periodically at 1s intervals as a speed of 1 m/s is assumed of indoor pedestrians. Hence, if the performance changes compared to the previous state, the optical receiver informs the controller via the feedback signal to update the RYGB LDs-light unit according to the SBA and PIA. If the time required to determine the value of each SNR in the SBA and PIA is equal to 1 ms, then the SBA training time is equal to 8 ms (8 RYGB LDs-light units × 1 ms) and the PIA requires 32 ms (8 iterations × 4 quadrants × 1 ms). Therefore, the adaptive CGH-VLC system can achieve 100% of the specified data rate when stationary and 96% in the case of a mobile user (i.e. 40 Gb/s for a stationary user and 38.4 Gb/s for a mobile user). It should be noted that users in an indoor environment, such as the one considered, are typically nomadic and therefore spend most of the time in one location, and as such achieve an average data rate near the maximum data rate supported. Table 2 illustrates the PIA algorithm.

C. MULTIPLE BEAMS GENERATION TECHNIQUE

Once the exact location of the receiver is found by PIA, the CGH algorithm generates the optimum number of beams that achieves a strong communication link between the transmitter and the receiver. It should be noted that due to the fact that each RYGB LDs-light unit has 9 RYGB LDs, the optimum number of beams generated varies from one to nine as each beam carries a different data stream. Later we will find the optimum number of beams by considering CCI. As an example, a desired far-field image pattern is shown in Fig. 8. To realize this far field pattern, the phase distribution of

TABLE 2. PIA algorithm.

Inputs:
j = 288 No. pf pixels of the imaging receiver.
$\theta_{x-start}$=-26.56° and θ_{x-end}=26.56° (the lower and higher scan ranges along x-axis).

$\theta_{y-start}$=-26.56° and θ_{y-end}=26.56° (the lower and higher scan ranges along y-axis).

Initial step size=100 cm (at the first iteration four quadrants should be scanned).

1. **for** i = -26.56:26.56:26.56;
2. **for** l = -26.56:26.56:26.56;
3. $\theta_x = i$; $\theta_y = l$; (Transmission angles in x and y axes)
4. Produce a beam with a direction associated with θ_x and θ_y.
5. **for** S =1: j;
6. Calculate and sum the received powers
7. Produce the impulse response $h_S(t)$
8. Calculate $(P_{S1} - P_{S0})$
9. Compute $SNR_S = (\frac{R(P_{S1}-P_{S0})}{\sigma_t})^2$;
10. **end for**
11. $SNR\,(i,l) = max\,(SNR_S)$;
12. **end for**
13. **end for**
14. $SNR_{max} = max\,SNR\,(i,l)$;
15. $[\theta_{x-best-qaudrant}, \theta_{y-best-qaudrant}] = find\,(SNR\,(i,l)) == (SNR_{max})$; (identify the best quadrant area).
16. **If** $|\theta_{x-best-quadrant}| \leq (|\theta_{x-end}| - |\theta_{x-start}|)/2$ (reset new scan range in the x-axis)
17. $\theta_{x-end} = \theta_{x-best-quadrant}$;
18. **Else**
19. $\theta_{x-start} = \theta_{x-best-quadrant}$;
20. **end If**
21. **If** $|\theta_{y-best-quadrant}| \leq (|\theta_{y-end}| - |\theta_{y-start}|)/2$ (reset new scan range in the y-axis)
22. $\theta_{y-end} = \theta_{y-best-quadrant}$;
23. **Else**
24. $\theta_{y-start} = \theta_{y-best-quadrant}$;
25. **end If**
26. $\theta_{x-best} = \theta_{x\text{-best-quadrant}}$; $\theta_{y-best} = \theta_{y\text{-best-quadrant}}$ (identify receiver location).

FIGURE 8. Desired beams in the far-field.

the CGH was gradually optimized by the simulated annealing algorithm (see Fig. 9). Fig. 9 illustrates three snapshots (iteration 1, 15 and 100) of the phase distribution of the

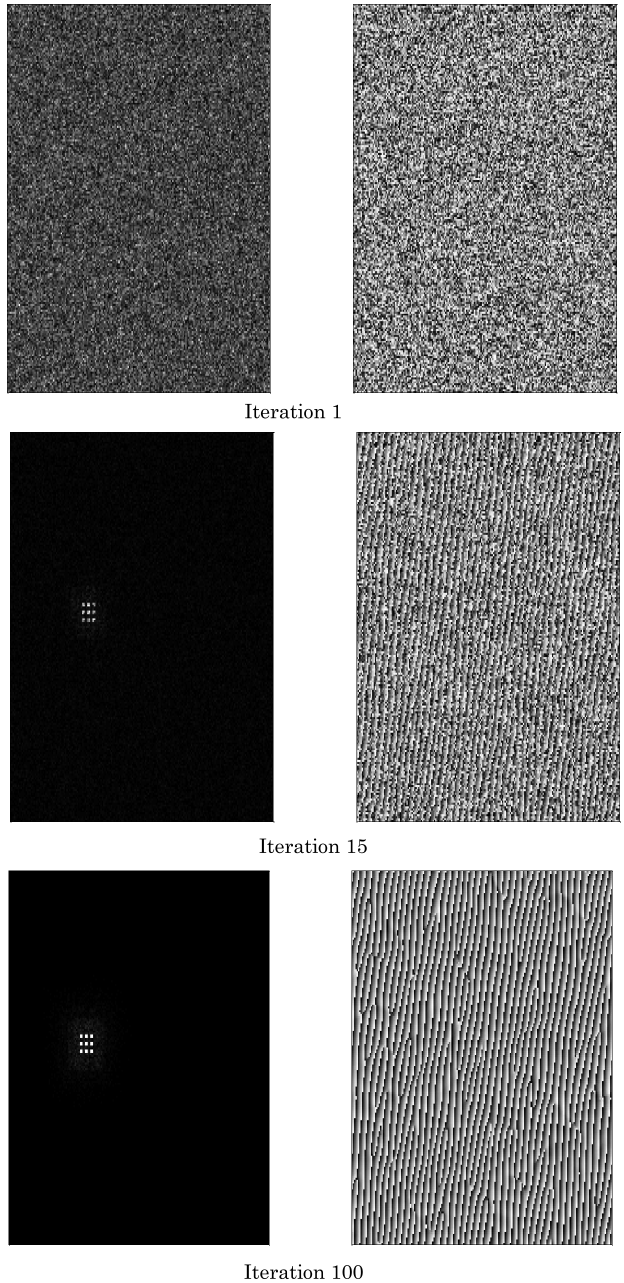

FIGURE 9. Phase distribution of the CGH (right hand) and the actual output pattern (left hand).

hologram and the image of the far-field pattern. It can be seen that by increasing the number of iterations, the desired far-field image is improved. This is due to the error (cost function) reduction through the simulated annealing algorithm as shown in Fig. 10. It should be noted that the optimization process is carried out before communication starts.

To find the optimum number of beams that to be generated by the CGH, we assume the bit error rate (BER) of each beam does not exceed 10^{-9}. In the adaptive CGH-VLC system, the CCI between beams was taken into account; hence, increasing the number of beams generated leads to increase

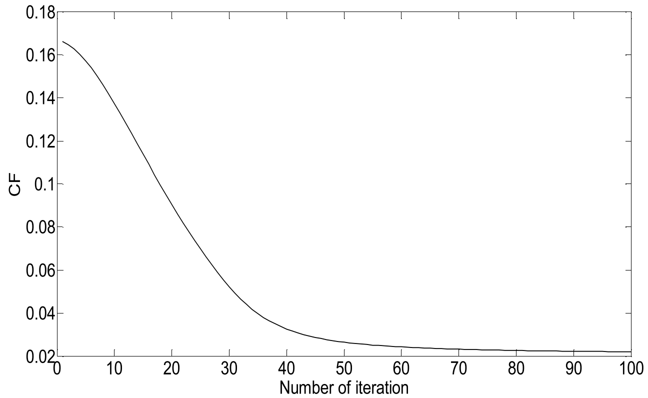

FIGURE 10. CF versus number of iterations.

in the CCI which degrades the system performance as each beam carries a different data. For OOK modulation, the BER can be given as [30]:

$$BER = Q\left(\sqrt{SINR}\right) \tag{13}$$

where $Q(x) = \frac{\int_x^{\infty} e^{-z^2/2}}{\sqrt{2\pi}}$ and $SINR$ is the signal to interference plus noise ratio. By considering ISI, the $SINR$ is expressed as [35], [42]:

$$SINR = \frac{R^2\left(P_{s1} - P_{s0}\right)^2}{\sigma t^2 + \sum_i^k \left(RP_i\right)^2} \tag{14}$$

where R is the photodetector's responsivity (0.4 A/W), (P_{s1}) is the received power associated with logic 1, (P_{s0}) is the received power associated with logic 0, σt is the total noise associated with the received signal, P_i is the interference power from the other beams and k is the number of beams. The total noise can be classified into three components and can be given as [43], [44]:

$$\sigma t = \sqrt{\sigma_{bn}^2 + \sigma_s^2 + \sigma_{pr}^2} \tag{15}$$

where σ_{bn} is the background shot noise component, σ_s is the shot noise component associated with the received signal and σ_{pr} is the preamplifier noise component. In this paper, we concider the effect of the three components of the niose. Calculation of the σ_{bn} and σ_s can be found in [30] and [36]. In addition, we used the p-i-n FET receiver designed in [45], which has an input noise current equal to 10 pA/$\sqrt{Hz}$.

To obtain the optimum number of beams that can be generated with BER not exceeding 10^{-9}, we placed the imaging receiver at the room centre (2 m, 4 m, 1 m) as the distance between the transmitters and the receiver is maximum at this location. We assumed the first beam generated is the desired beam and the other beams are the interfering beams. The $SINR$ and the BER were calculated for the desired beam at a data rate of 5 Gb/s with an increase in the number of interfering beams. In this work, the effect of reflections is considered. Hence, by increasing the number of beams, this leads to increase in the level of CCI due to reflections and degrades the performance of each beam. The results are shown in Table 3.

TABLE 3. Effect of the number of beams on the link performance.

Number of beams	SINR	BER
1	20.05	Error free
2	19.65	Error free
3	19.11	Error free
4	18.46	Error free
5	17.74	6.44×10^{-15}
6	16.98	8.29×10^{-13}
7	16.21	5.21×10^{-11}
8	15.63	0.75×10^{-9}
9	14.13	1.88×10^{-7}

As each RYGB LDs-light unit has 9 RYGB LDs, the CGH was utilized to generate up to 9 beams, and each beam carries a different data stream at the same data rate. It can be noted that the performance of the desired beam degrades when the number of the interfering beams is increased and this is attributed to the increase in the level of the CCI. As shown in Table 3, the optimum number of the beams is equal to 8, which gives BER not exceeding 10^{-9} given our system set up and parameters. Thus, the maximum data rate of our adaptive CGH-VLC system is 40 Gb/s (8 beams × 5 Gb/s). To find the pixels that received the data from each beam, each beam is given an ID. In the simulation, we set up a threshold in terms of $SINR$. Any pixel has $SINR$ less than 15.6 dB (BER more than 10^{-9}) was excluded. Hence, just the outputs of pixels that received data streams from beams enter to parallel to serial converter to obtain the data.

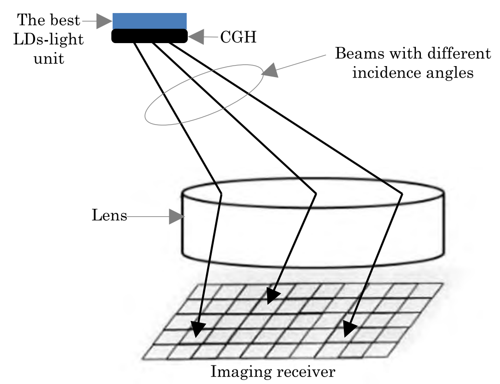

FIGURE 11. Imaging optical receiver with angular spatial mapping.

One of the main benefits of the imaging receiver is that each pixel can be treated as a single separate photodetector with narrow FOV, which can amplify the photocurrents received separately. Moreover, the imaging receiver has the ability to distinguish between signals that have a different incidence angle. This is due to the imaging receiver ability to perform angular-spatial mapping (each pixel has a very small acceptance angle), which means each received signal is focused onto a different pixel depending on the incidence angle of this signal as shown in Fig. 11 [46]. Therefore, the multiple beams were spatially separated by the CGH to give each beam a different incidence angle and each beam is received by a particular pixel (see Fig. 11). The lens has an entrance aperture with a diameter equal to 3 cm. Therefore, the separation between beams was adjusted based on this diameter. A requirement in our proposed system is the presence of an LOS component between the transmitter and the receiver. The system vulnerability to shadowing can be reduced by illumination each area using multiple light engine which warrants further research. It should be noted that the key benefit of the adaptive CGH-VLC system over the statistic CGH-VLC system is that all beams generated by the CGH are focused to the optical receiver. This leads to enhance 3-dB channel bandwidth, reduce path loss and increase received optical power. In addition, the adaptive CGH-VLC system tracks the optical receiver whenever the location of the optical receiver changes. The complexity in the design of the adaptive CGH-VLC system will be at the transmitter side. This is due to adding an extra device (i.e. the adaptive CGH) at the transmitter to find the receiver location and generated the beams. Therefore, the down link transmitters in the ceiling can be a quite bulky and expensive.

VII. SIMULATION RESULTS

The performance of the proposed systems in an empty room (room A) and a realistic room (room B) was evaluated. In this work, we used approach in [47] to produce the impulse response and hence determine the path loss, 3 dB channel bandwidth, the delay spread, SNR and SINR. A MATLAB program was used to obtain the results in this work. The proposed systems were investigated in many locations on the communication floor of the rooms. Table 4 gives the simulation parameters that were used in this work.

A. RESULTS OF THE STATIC CGH-VLC SYSTEM

We investigated the performance of the static CGH-VLC system in two different environments with the presence of diffusing reflections (up to second order) and mobility. In this system, we considered the single photodetector as an optical receiver and the results were obtained in terms of delay spread and SNR. It should be noted that just one RYGB LDs-light unit (the best RYGB LDs-light unit) was used to transmit the data and the static CGH that followed this transmitter was utilized to generate multiple beams (100 beams) on an area of 2 m × 2 m.

Due to non-directed transmission, indoor VLC systems are subject to multipath dispersion, which causes pulse spread in time. Delay spread is a good measure of signal pulse spread due to the temporal dispersion of the incoming signal. The delay spread of an impulse response is given by [37], [48]:

$$D = \sqrt{\frac{\sum_{i=-\infty}^{\infty} (t_i - \mu)^2 P_{ri}^2}{\sum_{i=-\infty}^{\infty} P_{ri}^2}} \quad (16)$$

where t_i is the delay time associated with the received optical power P_{ri} and μ is the mean delay given by:

$$\mu = \frac{\sum_{i=-\infty}^{\infty} t_i P_{ri}^2}{\sum_{i=-\infty}^{\infty} P_{ri}^2} \quad (17)$$

TABLE 4. Simulation parameters.

Parameters	Configurations	
Rooms		
Length	8 m	
Width	4 m	
Height	3 m	
ρ-xz Wall	0.8	
ρ-yz Wall	0.8	
ρ-xz op. Wall	0.8	
ρ-yz op. Wall	0.8	
ρ-Floor	0.3	
ρ-Windows	0	
ρ-Bookshelves	0.4	
Bounces	1	2
Number of elements	32000	2000
d_A	5 cm × 5 cm	20 cm×20 cm
Lambertian emission order (n)	1	
Sime-angle at half power	60°	
Transmitters		
Number of transmitters	8	
Locations(x, y, z) m	(1, 1, 3), (1, 3, 3), (1, 5, 3), (1, 7, 3), (3, 1, 3), (3, 3, 3), (3, 5, 3), (3, 7, 3)	
Number of RYGB LDs per unit	9 (3 × 3)	
RYGB LDs interval	0.03 m	
Transmitted Optical power/RYGB LD	1.9 W	
Centre luminous intensity	162 cd	
Lambertian emission order (n)	0.65	
Sime-angle at half power	70°	
Receivers		
Single photodetector		
Area of the photodetector	0.5mm²	
FOV	40°	
Responsivity	0.4 A/W	
Receiver's bandwidth	6.18 GHz	
Imaging receiver		
Concentrator entrance area	$\frac{9\pi}{4}$ cm²	
Concentrator refractive index	1.7	
Concentrator acceptance angle	65°	
Receiver's area	2 cm²	
Number of pixels	288	
Pixel's area	0.69 mm²	
Responsivity	0.4 A/W	
Receiver's bandwidth	4.48 GHz	

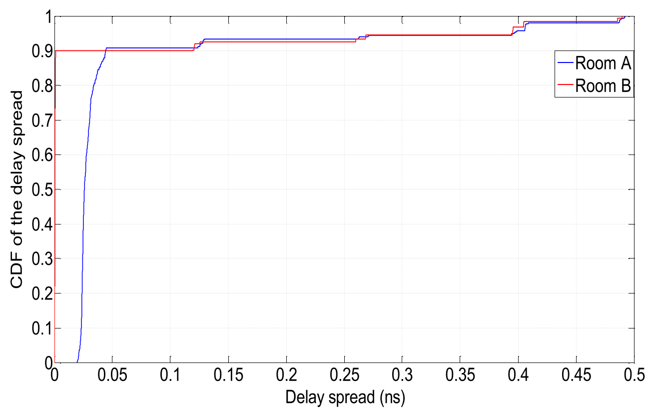

FIGURE 12. CDF of the delay spread of the static CGH-VLC system when the single photodetector was randomly placed in room A and in room B.

Fig. 12 shows the cumulative distribution function (CDF) of the delay spread of the static CGH-VLC system when the single photodetector was randomly located (500 random locations) on the communication floor of room A and room B.

It can be seen that the value of the delay spread is less than 0.05 ns for almost 91% of the total locations of the single photodetector in room A.On the other hand, 90% of the total locations of the single photodetector on the communication floor of room B has delay spread less than 0.0012 ns. This is due to two walls ($x = 0$ and $y = 0$) in room B which have windows with reflection coefficient equal to zero. In addition, two walls (wall $x = 4$ and wall $y = 8$) of room B are covered by bookshelves, which have reflection coefficients equal to 0.4. This leads to a reduction in the effect of the reflection components and consequently decrease the delay spread compared to room A.

In the static CGH-VLC system, all generated beams carried the same data; hence, there is no CCI. Thus, for this system, we obtained the SNR, which is given as [42]:

$$SNR = \left(\frac{R\,(P_{s1} - P_{s0})}{\sigma t} \right)^2 \tag{18}$$

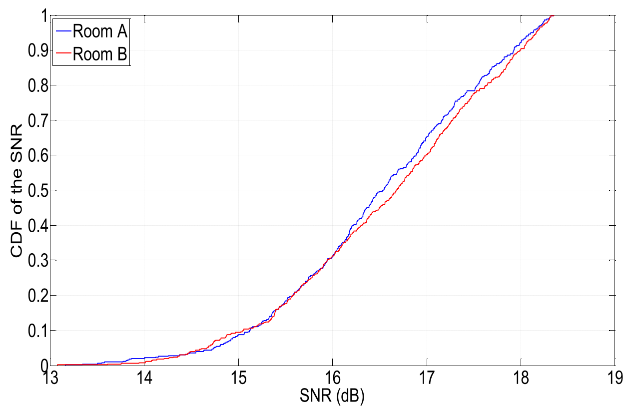

FIGURE 13. CDF of the SNR of the static CGH-VLC system when the system operates at 8 Gb/s and the single photodetector was randomly located in room A and in room B.

The CDF of the SNR for the static CGH-VLC system when the single photodetector is placed randomly on the communication floor of room A and room B is illustrated in Fig. 13. The SNR was obtained when the system operated at a data rate equal to 8 Gb/s. As seen in Fig. 13, at 80% of the locations, the static CGH-VLC system achieved a data rate of 8 Gb/s with SNR more than 15.6 dB (BER less than 10^{-9}). This system achieved an SNR between 13 dB and 15.6 dB at 20% of the total locations in room A and room B, with the 15.6 dB SNR supporting a data rate of 8 Gb/s at BER of 10^{-9}. For the 20% of locations with BER less than 10^{-9}, forward error correction codes can be used to reduce the BER to 10^{-9}.

B. PERFORMANCE EVALUATION OF THE ADAPTIVE CGH-VLC SYSTEM

The performance of the adaptive CGH-VLC system was evaluated when the imaging receiver was located along the y-axis of room A and room B. Due to the symmetry of room A, the results were obtained along the y-axis and at $x = 1$ m and $x = 2$ m while for room B, the results were examined when the imaging receiver was placed along the y-axis and at $x = 1$ m, $x = 2$ m and $x = 3$ m. In this system, each beam carries a different data stream at a rate of 5 Gb/s and the optimum number of beams that achieve a good communication link between the transmitter and the optical receiver (i.e. BER = 10^{-9} for each beam) was equal to eight, which enables the system to work at data rate of 40 Gb/s (8 beams × 5 Gb/s). Moreover, the results were displayed for one beam because of all beams have similar performance.

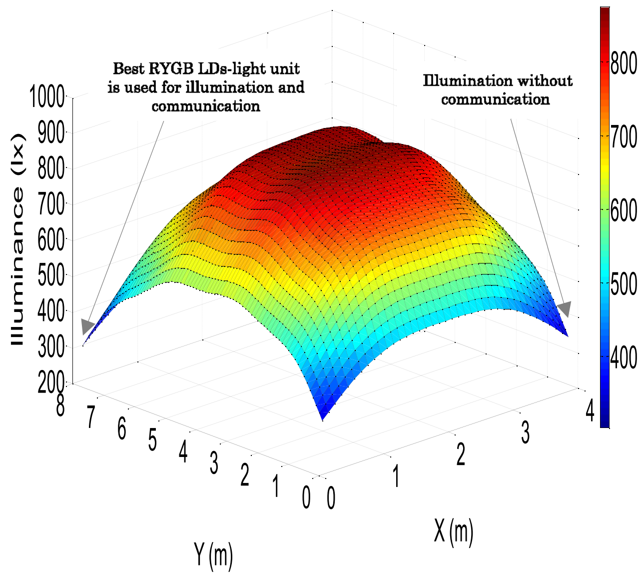

FIGURE 14. Distribution of the illumination of the adaptive CGH-VLC system on the communication floor; minimum illumination 303 lx and maximum illumination 874 lx.

It should be noted that just 20% of the total power of each RYGB LD in the best RYGB LDs-light unit was used to generate the beams in this system. To ensure that the illumination level stayed at an acceptable level in the room, Fig. 14 shows the distribution of the illumination in the room when the best RYGB LDs-light unit for communication was one of the light units at the room corner (the coordinates of the unit were 1 m, 7 m, 3 m), as the room corner has the lowest illumination level. As can be seen in Fig. 14, the illumination level achieved the minimum requirement for the illumination (i.e. 300 lx [28]).

1) OPTICAL PATH LOSS

Optical path loss is used to measure the attenuation of the transmitted beams, attributed to propagation in the free space and reflection components. Thus, the path loss is one of the main components that can help explain the VLC system's performance. The path loss (PL) is given as [49], [50]:

$$PL\,(dB) = -10 log_{10} \left(\int_{-\infty}^{\infty} h\,(t)\, dt \right) \tag{19}$$

where $h\,(t)$ is the impulse response.

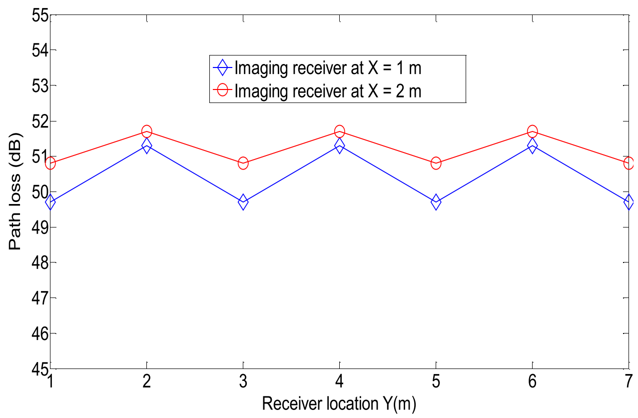

FIGURE 15. Path loss of the adaptive CGH-VLC system at different locations along the *y*-axis and at $x = 1$ m and $x = 2$ m in room A.

Fig. 15 illustrates the path loss of the adaptive CGH-VLC system (path loss of one beam) when the imaging receiver was located at $x = 1$ m and $x = 2$ m along the y-axis on the communication floor of room A. It can be seen that the lowest values of the path loss accrued when the receiver was placed near to the best RYGB LDs-light unit. Thus, the path loss along $x = 1$ m is better than $x = 2$ m since the receiver is close to the transmitters.

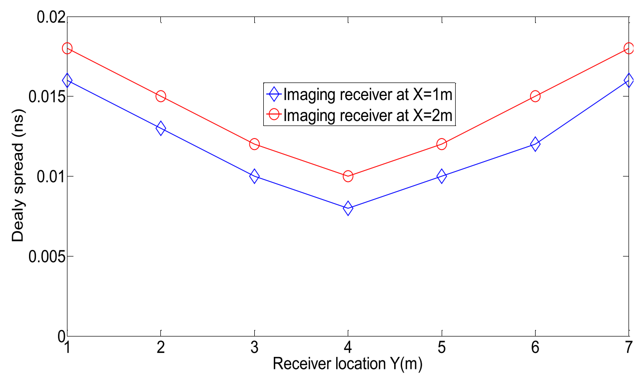

FIGURE 16. Delay spread of one beam of the adaptive CGH-VLC system at different locations along the *y*-axis and at $x = 1$ m and $x = 2$ m in room A.

2) DELAY SPREAD EVALUATION

Fig. 16 shows the delay spread of one beam of the adaptive CGH-VLC system at different locations of the imaging receiver along $x = 1$ m and $x = 2$ m. It can be seen that the worst case (the highest delay spread) for the proposed system was when the imaging receiver was located at the room edges. This is due to the delay spread being affected by the received power and delay time of the ray. Thus, the receiver is far from the walls $y = 8$ and $y = 0$, which means that the rays in the first and second reflections travel long distances at these locations. While, the best case for the delay spread (the lowest delay spread) for the designed system was when the imaging receiver was placed at the room center, due to the symmetry of room A and the optical receiver being close to all reflective surfaces of room A.

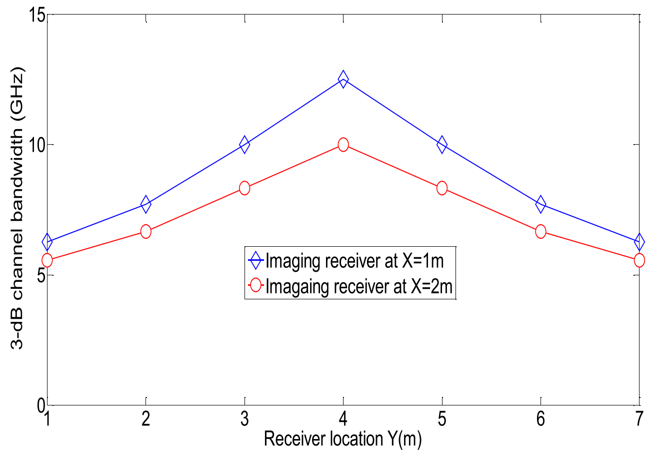

FIGURE 17. The 3 dB channel bandwidth of one beam of the adaptive CGH-VLC system at different locations of the imaging receiver along the *y*-axis and at $x = 1$ m and $x = 2$ m in room A.

3) 3 dB CHANNEL BANDWIDTH

The 3 dB channel bandwidth is an important factor in VLC systems, which is used to measure the ability of the VLC channel to support at a certain data rate. Fig. 17 shows the 3 dB channel bandwidth when the imaging receiver was located at different places of room A along the y-axis and at $x = 1$ m and $x = 2$ m. It can be seen that at all given locations of the imaging receiver on the communication floor of room A, the lowest 3 dB channel bandwidth of each produced beam in the best RYGB LDs-light unit was more than 5 GHz. Therefore, a high data rate (5 Gb/s) can be transmitted through each beam without ISI given that typically the bandwidth needed is 0.7 times the bit rate [34]. It should be noted that the results of the 3 dB channel bandwidth are in tandem with delay spread, e.g., when the optical receiver was at the center of the room, it had the lowest delay spread, which leads to the highest 3 dB channel bandwidth (see Figs. 18 and 19). Thus, the best value of the 3 dB channel bandwidth was when the user is located at the center of the room.

4) SINR OF THE ADAPTIVE CGH-VLC SYSTEM

Fig. 18 depicts the SINR of the adaptive CGH-VLC system when the imaging receiver is placed at a different location along the y-axis at $x = 1$ m and $x = 2$ m in room A. The SINR was obtained when each beam operated at 5 Gb/s. In this system, each beam from each RYGB LD in the best transmitter sends a different data stream at 5 Gb/s. It can be seen that at all proposed locations of the imaging receiver in room A, the value of the SINR of the beam offered a strong communication link at a high data rate of 5 Gb/s. Thus, the adaptive CGH-VLC system has the ability to achieve a high data rate of 40 Gb/s (8 beams $\times$ 5 Gb/s) with BER not

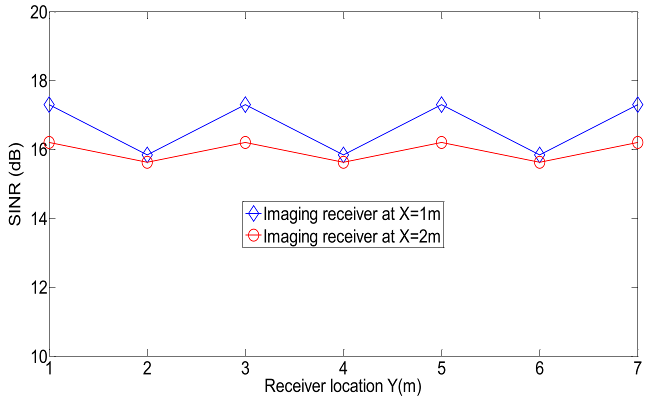

FIGURE 18. SINR of one beam of the adaptive CGH-VLC system at different locations of the imaging receiver along the *y*-axis and at $x = 1$ m and $x = 2$ m in room A when each beam operates at a data rate of 5 Gb/s.

exceeding 10^{-9}. Note that to get a data rate with BER not exceeding 10^{-9}, the SINR should not be less than 15.6 dB. Therefore, at some locations of the imaging receiver on the communication floor of room A (when the imaging receiver was located underneath of the best RYGB LDs-light unit) the data rate can be increased beyond 40 Gb/s. This is due to the high SINR (SINR = 17.3 dB) achieved at these locations.

5) EFFECTS OF BLOCKAGE AND SHADOWING ON ADAPTIVE CGH-VLC SYSTEM

To evaluate the effect of obstacles on the adaptive CGH-VLC system, the analysis was extended to the realistic room (room B). Due to the asymmetry of the realistic room, the imaging receiver was considered at different locations along the *y*-axis on the lines $x = 1$ m, $x = 2$ m and $x = 3$ m.

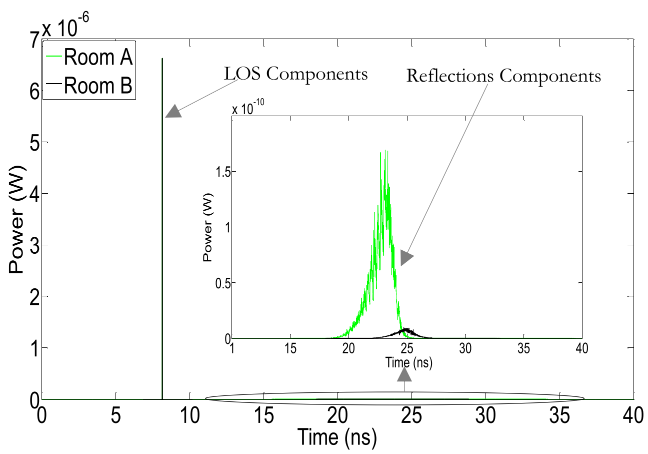

FIGURE 19. Impulse responses of the adaptive CGH-VLC system in two different environments when the imaging receiver is located at the center (2 m, 4 m, 1 m) of room A and room B.

Fig. 19 shows the impulse responses of one beam that was generated from the best RYGB LDs-light unit in two different room environments A and B when the imaging receiver was located at (2 m, 4 m, 1 m). As mentioned previously, LOS components have a great impact on VLC systems. Therefore, the performance of the adaptive CGH-VLC system was evaluated at all locations of the communication floor in room B, and it was found that our proposed system has the ability to establish LOS components at all locations. Thus, the LOS components of the proposed system in both room scenarios are equal, as shown in Fig. 19. On the other hand, the power collected from the reflection components (reflection components produced from the 80% of the total power of the best RYGB LDs-light unit) at the receiver side in room B were lower compared with room A (see Fig. 19), and this is due to several reasons. Firstly, in room B rays are prevented from reaching the imaging receiver by the physical partitions. Moreover, two walls ($x = 0$ and $y = 0$) in room B have windows that have a reflection coefficient of zero, which means that no signal will be reflected from them. In addition, in room B, two walls ($x = 4$ and $y = 8$) were covered with bookshelves with a reflectivity of 0.4, and consequently, the power reflected from these walls is reduced.

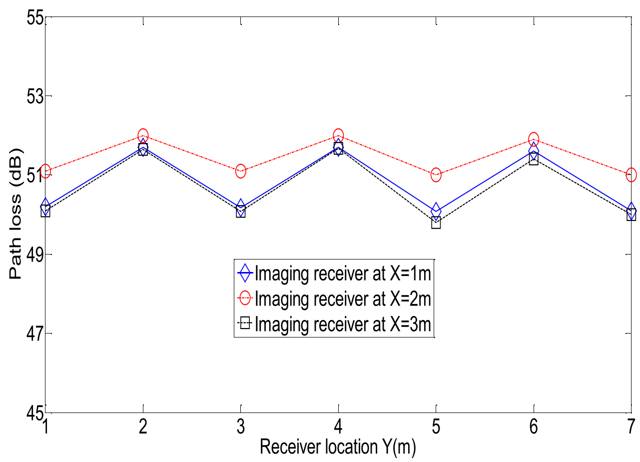

FIGURE 20. Path loss of one beam of the adaptive CGH-VLC system in room B when the imaging receiver was placed along the *y*-axis and at $x = 1$ m, $x = 2$ m and $x = 3$ m.

The path loss distribution of the adaptive CGH-VLC system in room B when the imaging receiver was placed along the *y*-axis at $x = 1$ m, $x = 2$ m and $x = 3$ m are illustrated in Fig. 20. It can be noted that the maximum path loss occurred when the imaging receiver was located along $x = 2$ m, and this is because of the distribution of the RYGB LDs-light units on the ceiling, which increases the distance to the maximum between the transmitters and the optical receiver along $x = 2$ m. As can be seen, when the imaging receiver is investigated along $x = 3$ m, the path loss was better (slightly lower) compared with that along $x = 1$ m. This is because along $x = 3$ m the closest walls (wall $x = 4$ and wall $y = 8$) to the optical receiver is covered by bookshelves with reflection coefficients of 0.4 while when the optical receiver was placed along $x = 1$ m, the closest walls ($x = 0$ and $y = 0$) has windows, which have zero reflection coefficients.

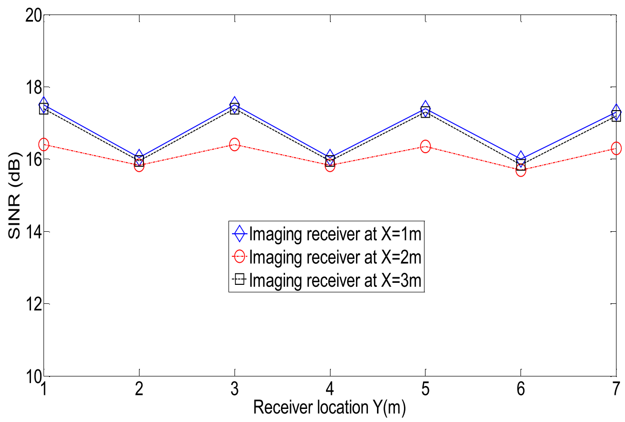

FIGURE 21. SINR of one beam of the adaptive CGH-VLC system in room B when the imaging receiver was placed along the *y*-axis and at $x = 1$ m, $x = 2$ m and $x = 3$ m when each beam operates at a data rate of 5 Gb/s.

TABLE 5. The BER of the of one beam of the CGH-VLC system in room B when the receiver is located at $x = 1$, $x = 2$ and $x = 3$.

Receiver locations along $x =$ 1 m	BER	Receiver locations along x = 2 m	BER	Receiver locations along x = 3 m	BER
1, 1, 1	4×10^{-14}	2, 1, 1	2×10^{-11}	3, 1, 1	7×10^{-14}
1, 2, 1	2×10^{-10}	2, 2, 1	3×10^{-10}	3, 2, 1	2×10^{-10}
1, 3, 1	4×10^{-14}	2, 3, 1	2×10^{-11}	3, 3, 1	7×10^{-14}
1, 4, 1	2×10^{-10}	2, 4, 1	3×10^{-10}	3, 4, 1	2×10^{-10}
1, 5, 1	4×10^{-14}	2, 5, 1	2×10^{-11}	3, 5, 1	7×10^{-14}
1, 6, 1	2×10^{-10}	2, 6, 1	3×10^{-10}	3, 6, 1	2×10^{-10}
1, 7, 1	4×10^{-14}	2, 7, 1	2×10^{-11}	3, 7, 1	7×10^{-14}

Fig. 21 shows the SINR of the adaptive CGH-VLC system in the realistic room for different locations of the imaging receiver along the y-axis at $x = 1$ m, $x = 2$ m and $x = 3$ m. The lowest values of the SINR occurred when the receiver was located along the y-axis at $x = 2$ m. The SINR of the system when the optical receiver was located along the y-axis at $x = 1$ m and $x = 3$ m are comparable as shown in Fig. 21. However, the SINR along $x = 1$ m is slightly higher than the SINR along $x = 3$ m. This is due to the presence of the windows, which have zero reflection coefficients, when the imaging receiver was placed along $x = 1$ m, while the bookshelves, which have 0.4 reflection coefficient, are close to the receiver when it was located along $x = 3$ m. Consequently, along $x = 1$ m the reflection components are minimal, which leads to enhanced system performance.

The BER of one beam of the adaptive CGH-VLC system when the imaging receiver was located at different locations on the communication floor of room B along the y-axis at $x = 1$ m, $x = 2$ m and $x = 3$ m and when each beam carried a data rate of 5 Gb/s are given in Table 5. It can be seen that the maximum value of the BER of the proposed system is 3×10^{-10}, which can achieve a high data rate (5 Gb/s for each beam) with a strong communication link.

It should be noted that the CGH redirects the generated beams to the optical receiver whenever the location of the receiver changes. As seen in Table 5, the BER is lower when the optical receiver moves along $x = 1$ m and $x = 3$ m compared with $x = 2$ m. This is due to the fact that along $x = 2$ m, the distance between the transmitters and the optical receiver are higher compared with the distances when the imaging receiver moves along $x = 1$ m and $x = 3$ m, which leads to a reduced received optical power and consequently increased BER along $x = 2$ m. Furthermore, the BER can change despite beam steering when the position of the imaging receiver is changed if the beams are broad and are not fully collected by the reveiver pixel.

VIII. CONCLUSIONS

Two indoor VLC systems based on a CGH were presented in this paper, a simple static CGH-VLC system and an adaptive CGH-VLC system. The CGH is used to direct a part of the total power of the best RYGB LDs-light unit, generate multiple beams and focus these beams on a specific area on the communication floor of the room. In the static CGH-VLC system, the CGH is utilized to direct 30% of the total power of the best transmitter, to generate 100 beams and to direct these beams on an area of 2 m × 2 m. All generated beams transmitted the same data, and the 30% was selected to ensure that the illumination stayed at the level required by standards. The static CGH-VLC system was able to achieve a data rate of 8 Gb/s while using a single photodetector and considering the influence of the reflections (up to second order) and mobility of the optical receiver. This system is, therefore, a low complexity (static hologram, single receiver) relatively high data rate (8 Gb/s) system. On the other hand, the CGH was used in the adaptive CGH-VLC system to direct 20% of the total power of the best RYGB LDs-light unit, generate eight beams (optimum number of beams dictated by CCI) and steer these beams to the imaging receiver. Each generated beam conveyed a different data stream at a rate of 5 Gb/s. The CCI between beams was taken into account in this system as the beams conveyed different data streams. The adaptive CGH-VLC system offered a data rate of 40 Gb/s (8 beams × 5 Gb/s) with BER not going below 10^{-9}.

REFERENCES

[1] A. M. Khalid, G. Cossu, R. Corsini, P. Choudhury, and E. Ciaramella, "1-Gb/s transmission over a phosphorescent white LED by using rate-adaptive discrete multitone modulation," *IEEE Photon. J.*, vol. 4, no. 5, pp. 1465–1473, Oct. 2012.

[2] A. T. Hussein and J. M. H. Elmirghani, "High-speed indoor visible light communication system employing laser diodes and angle diversity receivers," in *Proc. 17th Int. Conf. Transp. Opt. Netw. (ICTON)*, Jul. 2015, pp. 1–6.

[3] L. Zeng *et al.*, "High data rate multiple input multiple output (MIMO) optical wireless communications using white LED lighting," *IEEE J. Sel. Areas Commun.*, vol. 27, no. 9, pp. 1654–1662, Dec. 2009.

[4] A. T. Hussein and J. M. H. Elmirghani, "Mobile multi-gigabit visible light communication system in realistic indoor environment," *J. Lightw. Technol.*, vol. 33, no. 15, pp. 3293–3307, Aug. 1, 2015.

[5] L. Zeng, D. O'Brien, H. Le-Minh, K. Lee, D. Jung, and Y. Oh, "Improvement of date rate by using equalization in an indoor visible light communication system," in *Proc. 4th IEEE Int. Conf. Circuits Syst. Commun.*, May 2008, pp. 678–682.

[6] H. Le Minh *et al.*, "High-speed visible light communications using multiple-resonant equalization," *IEEE Photon. Technol. Lett.*, vol. 20, no. 14, pp. 1243–1245, Jul. 15, 2008.

[7] H. Le Minh *et al.*, "80 Mbit/s visible light communications using pre-equalized white LED," in *Proc. 34th Eur. Conf. Opt. Commun.*, Sep. 2008, pp. 1–2.

[8] J. Grubor, S. C. J. Lee, K.-D. Langer, T. Koonen, and J. W. Walewski, "Wireless high-speed data transmission with phosphorescent white-light LEDs," in *Proc. ECOC*, Sep. 2007, pp. 1–2.

[9] A. H. Azhar, T.-A. Tran, and D. O'Brien, "Demonstration of high-speed data transmission using MIMO-OFDM visible light communications," in *Proc. GLOBECOM Workshops (GC Wkshps)*, Dec. 2010, pp. 1052–1056.

[10] J. Vučić, C. Kottke, S. Nerreter, K.-D. Langer, and J. W. Walewski, "513 Mbit/s visible light communications link based on DMT-modulation of a white LED," *J. Lightw. Technol.*, vol. 28, no. 24, pp. 3512–3518, Dec. 15, 2010.

[11] H. Chun *et al.*, "LED based wavelength division multiplexed 10 Gb/s visible light communications," *J. Lightw. Technol.*, vol. 34, no. 13, pp. 3047–3052, Jul. 1, 2016.

[12] G. Cossu, W. Ali, R. Corsini, and E. Ciaramella, "Gigabit-class optical wireless communication system at indoor distances (1.5–4 m)," *Opt. Exp.*, vol. 23, no. 12, pp. 15700–15705, 2015.

[13] L. Cui, Y. Tang, H. Jia, J. Luo, and B. Gnade, "Analysis of the multichannel WDM-VLC communication system," *J. Lightw. Technol.*, vol. 34, no. 24, pp. 5627–5634, Dec. 15, 2016.

[14] C. Lee *et al.*, "4 Gbps direct modulation of 450 nm GaN laser for high-speed visible light communication," *Opt. Exp.*, vol. 23, no. 12, pp. 16232–16237, Jun. 2015.

[15] H. Chun, S. Rajbhandari, D. Tsonev, G. Faulkner, H. Haas, and D. O'Brien, "Visible light communication using laser diode based remote phosphor technique," in *Proc. Int. Conf. Commun. Workshop (ICCW)*, Jun. 2015, pp. 1392–1397.

[16] S. H. Younus and J. M. H. Elmirghani, "WDM for high-speed indoor visible light communication system," in *Proc. 19th Int. Conf. Transp. Opt. Netw. (ICTON)*, Jul. 2017, pp. 1–6.

[17] D. Tsonev, S. Videv, and H. Haas, "Towards a 100 Gb/s visible light wireless access network," *Opt. Exp.*, vol. 23, no. 2, pp. 1627–1637, Jan. 2015.

[18] F. E. Alsaadi and J. M. H. Elmirghani, "High-speed spot diffusing mobile optical wireless system employing beam angle and power adaptation and imaging receivers," *J. Lightw. Technol.*, vol. 28, no. 16, pp. 2191–2206, Aug. 10, 2010.

[19] M. T. Alresheedi and J. M. H. Elmirghani, "Performance evaluation of 5 Gbit/s and 10 Gbit/s mobile optical wireless systems employing beam angle and power adaptation with diversity receivers," *IEEE J. Sel. Areas Commun.*, vol. 29, no. 6, pp. 1328–1340, Jun. 2011.

[20] S.-M. Kim and S.-M. Kim, "Performance improvement of visible light communications using optical beamforming," in *Proc. 5th Int. Conf. Ubiquitous Future Netw. (ICUFN)*, Jul. 2013, pp. 362–365.

[21] A. T. Hussein, M. T. Alresheedi, and J. M. H. Elmirghani, "20 Gb/s mobile indoor visible light communication system employing beam steering and computer generated holograms," *J. Lightw. Technol.*, vol. 33, no. 24, pp. 5242–5260, Dec. 15, 2015.

[22] A. T. Hussein, M. T. Alresheedi, and J. M. H. Elmirghani, "Fast and efficient adaptation techniques for visible light communication systems," *J. Opt. Commun. Netw.*, vol. 8, no. 6, pp. 382–397, Jun. 2016.

[23] F. R. Gfeller and U. Bapst, "Wireless in-house data communication via diffuse infrared radiation," *Proc. IEEE*, vol. 67, no. 11, pp. 1474–1486, Nov. 1979.

[24] M. T. Alresheedi and J. M. H. Elmirghani, "Hologram selection in realistic indoor optical wireless systems with angle diversity receivers," *J. Opt. Commun. Netw.*, vol. 7, no. 8, pp. 797–813, 2015.

[25] A. T. Hussein and J. M. H. Elmirghani, "10 Gbps mobile visible light communication system employing angle diversity, imaging receivers, and relay nodes," *J. Opt. Commun. Netw.*, vol. 7, no. 8, pp. 718–735, 2015.

[26] M. P. Carolus, M. Krijn, and M. J. J. Jak, "Eye-safe laser-based lighting," Google Patents 2011 0 116 520, May 19, 2011.

[27] A. Neumann, J. J. Wierer, W. Davis, Y. Ohno, S. R. J. Brueck, and J. Y. Tsao, "Four-color laser white illuminant demonstrating high color-rendering quality," *Opt. Exp.*, vol. 19, no. 104, pp. A982–A990, 2011.

[28] *European Standard EN 12464-1: Lighting of Indoor Work Places*. Accessed: Jan. 2, 2015. [online]. Available: http://www.etaplighting.com/upoadedFiles/Downloadable_documentation/documentatie/EN12464_E_OK.pdf

[29] T. Komine and M. Nakagawa, "Fundamental analysis for visible-light communication system using LED lights," *IEEE Trans. Consum. Electron.*, vol. 50, no. 1, pp. 100–107, Feb. 2004.

[30] J. M. Kahn and J. R. Barry, "Wireless infrared communications," *Proc. IEEE*, vol. 85, no. 2, pp. 265–298, Feb. 1997.

[31] T. Shang, T. Jiang, Y. T. Yang, P. Wang, and Y. Liu, "Multi-users network model and the corresponding networking scheme for indoor VLC systems," *Opt. Exp.*, vol. 23, no. 9, pp. 11600–11618, 2015.

[32] *Photodiode Tutorial*. Accessed: Jan. 2017. [Online]. Available: https://www.thorlabs.com/tutorials.cfm?tabID=787382ff-26eb4a7e-b021-bf65c5bf164b

[33] A. P. Tang, J. M. Kahn, and K.-P. Ho, "Wireless infrared communication links using multi-beam transmitters and imaging receivers," in *Proc. ICC*, Jun. 1996, pp. 180–186.

[34] S. D. Personick, "Receiver design for digital fiber optic communication systems, I," *Bell Syst. Tech. J.*, vol. 52, no. 6, pp. 843–874, Jul. 1973.

[35] P. Djahani and J. M. Kahn, "Analysis of infrared wireless links employing multibeam transmitters and imaging diversity receivers," *IEEE Trans. Commun.*, vol. 48, no. 12, pp. 2077–2088, Dec. 2000.

[36] M. T. Alresheedi and J. M. H. Elmirghani, "10 Gb/s indoor optical wireless systems employing beam delay, power, and angle adaptation methods with imaging detection," *J. Lightw. Technol.*, vol. 30, no. 12, pp. 1843–1856, Jun. 15, 2012.

[37] S. T. Jovkova and M. Kavehard, "Multispot diffusing configuration for wireless infrared access," *IEEE Trans. Commun.*, vol. 48, no. 6, pp. 970–978, Jun. 2000.

[38] M. A. Seldowitz, J. P. Allebach, and D. W. Sweeney, "Synthesis of digital holograms by direct binary search," *Appl. Opt.*, vol. 26, no. 14, pp. 2788–2798, 1987.

[39] P. Carnevali, L. Coletti, and S. Patarnello, "Image processing by simulated annealing," *IBM J. Res. Develop.*, vol. 29, no. 6, pp. 569–579, 1985.

[40] M. T. Alresheedi, A. T. Hussein, and J. M. H. Elmirghani, "Uplink design in VLC systems with IR sources and beam steering," *IET Commun.*, vol. 11, no. 3, pp. 311–317, 2017.

[41] F. E. Alsaadi, M. A. Alhartomi, and J. M. H. Elmirghani, "Fast and efficient adaptation algorithms for multi-gigabit wireless infrared systems," *J. Lightw. Technol.*, vol. 31, no. 23, pp. 3735–3751, Dec. 1, 2013.

[42] A. G. Al-Ghamdi and J. M. H. Elmirghani, "Line strip spot-diffusing transmitter configuration for optical wireless systems influenced by background noise and multipath dispersion," *IEEE Trans. Commun.*, vol. 52, no. 1, pp. 37–45, Jan. 2004.

[43] F. Alsaadi and J. M. H. Elmirghani, "Mobile multigigabit indoor optical wireless systems employing multibeam power adaptation and imaging diversity receivers," *J. Opt. Commun. Netw.*, vol. 3, no. 1, pp. 27–39, Jan. 2011.

[44] I. Stefan, H. Elgala, and H. Haas, "Study of dimming and LED nonlinearity for ACO-OFDM based VLC systems," in *Proc. Wireless Commun. Netw. Conf. (WCNC)*, Apr. 2012, pp. 990–994.

[45] E. M. Kimber, B. L. Patel, I. Hardcastle, and A. Hadjifotiou, "High performance 10 Gbit/s pin-FET optical receiver," *Electron. Lett.*, vol. 28, no. 2, pp. 120–122, Jan. 1992.

[46] S. Jivkova and M. Kavehrad, "Transceiver design concept for cellular and multispot diffusing regimes of transmission," *EURASIP J. Wireless Commun. Netw.*, vol. 2005, no. 1, pp. 30–38, 2005.

[47] J. R. Barry, J. M. Kahn, W. J. Krause, E. A. Lee, and D. G. Messerschmitt, "Simulation of multipath impulse response for indoor wireless optical channels," *IEEE J. Sel. Areas Commun.*, vol. 11, no. 3, pp. 367–379, Apr. 1993.

[48] A. G. Al-Ghamdi and J. M. H. Elmirghani, "Analysis of diffuse optical wireless channels employing spot-diffusing techniques, diversity receivers, and combining schemes," *IEEE Trans. Commun.*, vol. 52, no. 10, pp. 1622–1631, Oct. 2004.

[49] A. G. Al-Ghamdi and J. M. H. Elmirghani, "Performance comparison of LSMS and conventional diffuse and hybrid optical wireless techniques in a real indoor environment," *IEE Proc.-Optoelectron.*, vol. 152, no. 4, pp. 230–238, Aug. 2005.

[50] M. R. Pakravan and M. Kavehrad, "Design considerations for broadband indoor infrared wireless communication systems," *Int. J. Wireless Inf. Netw.*, vol. 2, no. 4, pp. 223–238, 1995.

SAFWAN HAFEEDH YOUNUS received the B.Sc. degree in electronic and electrical engineering and the M.Sc. degree (Hons.) in communication systems from the University of Mosul, Iraq, in 2008 and 2010, respectively. He is currently working toward the Ph.D. degree at the School of Electronic and Electrical Engineering, University of Leeds, Leeds, U.K. From 2010 to 2012, he was a Maintenance and Support Engineer of the NGN local network at the Ministry of Communication, Iraq. He was a Lecturer at the Communication Department, College of Electronics, University of Mosul, from 2012 to 2014. He is currently a Scholar at the Ministry of Higher Education and Scientific Research, Iraq. His research interests include performance enhancement techniques for visible light communication systems, visible light communication system design, and indoor visible light communication networking.

AHMED TAHA HUSSEIN received the B.Sc. degree (Hons.) in electronic and electrical engineering and the M.Sc. degree (Hons.) in communication systems from the University of Mosul, Iraq, in 2006 and 2011, respectively, and the Ph.D. degree in visible light communication systems from the University of Leeds, Leeds, U.K., in 2017. He was a Communication Instructor at the Electronic and Electrical Engineering Department, College of Engineering, University of Mosul, from 2006 to 2009, where he was a Lecturer at the Electronic and Electrical Engineering Department, from 2011 to 2012. He has authored widely in the top IEEE communications conferences and journals. His research interests include performance enhancement techniques for visible light communication systems, visible light communication system design, and indoor visible light communication networking. He received the Carter Award from the University of Leeds for the best journal.

MOHAMMED THAMER ALRESHEEDI received the B.Sc. degree (Hons.) in electrical engineering from King Saud University, Riyadh, Saudi Arabia, in 2006 and the M.Sc. degree (Hons.) in communication engineering and the Ph.D. degree in electronic and electrical engineering from the University of Leeds, Leeds, U.K., in 2009 and 2014, respectively. He is currently an Assistant Professor at the Department of Electrical Engineering, King Saud University. His research interests include adaptive techniques for optical wireless (OW), OW systems design, indoor OW networking, and visible light communications.

JAAFAR M. H. ELMIRGHANI (M'92–SM'99) received the B.Sc. degree in electrical engineering (First Class Honors) from the University of Khartoum in 1989 and was awarded all four prizes in the department for academic distinction. He received the Ph.D. degree in the synchronization of optical systems and optical receiver design from the University of Huddersfield, U.K., in 1994 and the D.Sc. degree in communication systems and networks from University of Leeds, U.K., in 2014. He is the Director of the Institute of Integrated Information Systems within the School of Electronic and Electrical Engineering, University of Leeds, U.K. He joined the University of Leeds in 2007 and prior to that (2000–2007) as Chair in Optical Communications at the University of Wales Swansea he founded, developed, and directed the Institute of Advanced Telecommunications and the Technium Digital (TD), a technology incubator/spinoff hub. He has provided outstanding leadership in a number of large research projects at the IAT and TD. He has coauthored *Photonic Switching Technology: Systems and Networks* (Wiley) and has published over 450 papers. He has research interests in optical systems and networks. Prof. Elmirghani is Fellow of the IET, Chartered Engineer, and Fellow of the Institute of Physics. He was Chairman of IEEE Comsoc Transmission Access and Optical Systems Technical Committee and was Chairman of IEEE Comsoc Signal Processing and Communications Electronics Technical Committee, and an editor of *IEEE Communications Magazine*. He was founding Chair of the Advanced Signal Processing for Communication Symposium which started at IEEE GLOBECOM'99 and has continued since at every ICC and GLOBECOM. He was also founding Chair of the first IEEE ICC/GLOBECOM optical symposium at GLOBECOM'00, the Future Photonic Network Technologies, Architectures and Protocols Symposium. He chaired this Symposium, which continues to date under different names. He was the founding Chair of the first Green Track at ICC/GLOBECOM at GLOBECOM 2011, and is Chair of the IEEE Green ICT initiative within the IEEE Technical Activities Board (TAB) Future Directions Committee (FDC), a pan IEEE Societies initiative responsible for Green ICT activities across IEEE, 2012-present. He is and has been on the technical program committee of 35 IEEE ICC/GLOBECOM conferences between 1995 and 2017 including 16 times as Symposium Chair. He has given over 55 invited and keynote talks over the past 8 years. He received the IEEE Communications Society Hal Sobol award, the IEEE Comsoc Chapter Achievement award for excellence in chapter activities (both in international competition in 2005), the University of Wales Swansea Outstanding Research Achievement Award, 2006; and received in international competition: the IEEE Communications Society Signal Processing and Communication Electronics outstanding service award, 2009, a best paper award at IEEE ICC'2013. Related to Green Communications he received the IEEE Comsoc Transmission Access and Optical Systems outstanding Service award 2015 in recognition of "Leadership and Contributions to the Area of Green Communications," the GreenTouch 1000x award in 2015 for "pioneering research contributions to the field of energy efficiency in telecommunications," the IET 2016 Premium Award for best paper in *IET Optoelectronics*, and shared the 2016 Edison Award in the collective disruption category with a team of 6 from GreenTouch for their joint work on the GreenMeter. He is currently an editor of IET Optoelectronics and *Journal of Optical Communications*, an was editor of IEEE Communications Surveys and Tutorials and IEEE Journal on Selected Areas in Communications series on Green Communications and Networking. He was Co-Chair of the GreenTouch Wired, Core and Access Networks Working Group, an adviser to the Commonwealth Scholarship Commission, member of the Royal Society International Joint Projects Panel and member of the Engineering and Physical Sciences Research Council (EPSRC) College. He has been awarded in excess of £22 million in grants to date from EPSRC, the EU, and industry, and has held prestigious fellowships funded by the Royal Society and by BT. He was an IEEE Comsoc Distinguished Lecturer 2013-2016.